Coherence in Complex Networks of Oscillators

Pedro G. Lind[1,2], Jason A.C. Gallas[1,3], and Hans J. Herrmann[1,4]

[1] ICP, Universität Stuttgart, Pfaffenwaldring 27, D-70569 Stuttgart, Germany
[2] Centro de Física Teórica e Computacional, Av. Prof. Gama Pinto 2, 1649-003 Lisbon, Portugal
[3] Instituto de Física, Universidade Federal do Rio Grande do Sul, 91501-970 Porto Alegre, Brazil
[4] Departamento de Física, Universidade Federal do Ceará, 60451-970 Fortaleza, Brazil

Summary. We study fully synchronized (coherent) states in complex networks of chaotic oscillators, reviewing the analytical approach of determining the stability conditions for synchronizability and comparing them with numerical criteria. As an example, we present detailed results for networks of chaotic logistic maps having three different scale-free topologies: random scale-free topology, deterministic pseudo-fractal scale-free network and Apollonian network. For random scale-free topology we find that the lower boundary of the synchronizability region scales approximately as $k^{-\mu}$, where k is the outgoing connectivity and μ depends on the local nonlinearity. For deterministic scale-free networks coherence is observed only when the coupling is heterogeneous, namely when it is proportional to some power of the neighbour connectivity. In all cases, stability conditions are determined from the eigenvalue spectrum of the Laplacian matrix and agree well with numerical results based on histograms of coherent states in parameter space. Additionally, we show that almost everywhere in the synchronizability region the basin of attraction of the coherent states fills the entire phase space, and that the transition to coherence is of first-order.

1 The Interplay Between Dynamics and Topology

The structure and dynamics underlying complex networks have been widely investigated, providing insight for many systems where they arise naturally [1–3]. Complex networks appear in a wide variety of fields ranging from lasers [4], granular media [5, 6], quantum transport [7], colloidal suspensions [8], electrical circuits [9], and time series analysis [10], to heart rhythms [11], epidemics [12, 13], protein folding [14], and locomotion [15] among others [1–3].

From the mathematical point of view, a network is a graph, composed by nodes or vertices and by their connections or edges [2]. Sometimes, each node is characterized by some dynamical state (amplitude), which evolves according to some local contribution and to the interaction with the neighbourhood. In other words, the complexity of the system underlying the network may be introduced either in the way nodes are interconnected (topology) or in the way nodes evolve in time (dynamics).

When studying network dynamics one frequently assumes a regular topology (lattice) where each node evolves according to some more or less complicated dynamics, typically fixed points [16], limit cycles [17] or chaotic attractors [18,19]. One main goal of this approach is to study the so-called spatio-temporal chaos which appears in many different spatially extended systems out of equilibrium, such as hydrodynamical flows, chemical reactions and biological systems [20,21]. Two main topics in this context concern the study of mechanisms underlying pattern formation and pattern selection [20–24] and also the study of chaotic synchronization behaviour [16,25].

Spatially extended systems are fundamentally modelled by (i) sets of coupled differential equations [20] with nonlinear terms, where both time and amplitude are continuous, (ii) cellular automata [22], where both time and amplitude are discrete or (iii) coupled map lattices [21], where time is discrete as in cellular automata, but where the space of states is continuous. In all these models the underlying networks have connections whose range assumes all values from 1 (nearest neighbours) up to some maximum range, in particular the size of the system (global coupling regime). In other words, neglecting boundary conditions, these network systems assume translational symmetry and therefore the underlying network is called a regular network.

To study more complicated network structures, one usually neglects node dynamics and all complexity is introduced by the network topology, i.e. by the way nodes are connected to each other. This can be done in three different ways [2]: by randomly connecting the nodes (random networks [26,27]), by considering some random long-range connections in a regular network with some small range of couplings (small-world networks [28,29]), or by considering the introduction of new nodes which are connected to the previous ones following some rule of preferential attachment (scale-free networks [30]). For all these cases there is no translational symmetry and no typical range connection: connections do not have any 'spatial' interpretation. Therefore, one uses some general topological quantities to characterize each particular network, namely the average path length $\langle \ell \rangle$, i.e. the average minimum number of connections linking two nodes, the clustering coefficient C, defined as the average fraction of neighbours which are connected to each other, and the distribution of connections $P(k)$, representing the number of nodes having k connections. Table 1 shows the values of these three quantities for all three topologies.

Random networks were introduced by Erdös and Rényi in the late fifties [26] to study organizing principles underlying some real networks [27]. In random networks one defines some probability $p(N)$ for any two nodes to be connected in a total of N nodes. Consequently, the connections are typically long-range connections having a completely irregular structure. One main goal in studying random networks is to determine the critical probability $p_c(N)$, beyond which some specific property is very likely to be observed, e.g. the critical probability marking a transition to percolation [31]. One

Table 1. Characterizing complex topologies with the topological quantities: average path length $\langle \ell \rangle$, clustering coefficient C and distributions $P(k)$ of connections k. Here N is the total number of nodes, p is the probability for two nodes to be connected, $\bar{k}$ is the average number of connections per node, C_0 is the clustering coefficient of the regular network from which the small-world network is constructed, and m is the number of initial connections of each new node in a scale-free network

	Random	Small-world	Scale-free
$\langle \ell \rangle$	$\ln N / \ln(pN)$	N for small p $\ln N$ for large p	$\ln N / \ln \ln N$
C	$\bar{k}/N$	$C_0(1-p)^3$	$\sim N^{-3/4}$
$P(k)$	$\mathrm{e}^{-\bar{k}}\bar{k}^k/k!$	$\mathrm{e}^{-\bar{k}}\bar{k}^k/k!$	$2m^2/k^3$

important feature of random networks, which also appears in real networks, is their small average path length $\langle \ell \rangle$, i.e. the average distance between any two nodes increases slowly with the system size. However, unlike random networks, real networks also have large cluster coefficients C.

Small-world networks were introduced recently by Watts and Strogatz [28] in order to implement both short $\langle \ell \rangle$ and large C features. Small-world networks have short-range connections between neighbours, as in regular networks, but they also have long-range connections similar to random networks, without middle range ones. There are mainly two procedures to construct a small-world network: starting from the same regular network, where each site is coupled to some number of first neighbours, one either *rewires* each regular connection with probability p (Watts–Strogatz model [28]) or *adds* a random connection to each node with probability p (Newman–Watts model [32]). The second procedure is more appropriate for most purposes, since it avoids the possibility of generating disconnected clusters [32].

Both random and small-world topologies produce typically networks where connections obey a Poisson distribution (see Table 1). However, there are real systems which are scale-free, i.e. where the connection distribution obeys a power law.

Scale-free networks were introduced by Barabási and Albert [30] using growing and preferential attachment: one starts with a small amount of fully interconnected nodes, and adds iteratively one node with m connections to the previous nodes, chosen from a probability function proportional to their number of connections. With this construction one obtains analytically [33–36] a distribution of the connections $P(k) \propto k^{-\gamma}$, where $\gamma \to 3$ as $N \to \infty$, independently of the initial number of fully interconnected nodes and of m. It is also possible to generate scale-free networks, either by imposing *a priori* a power-law distribution of all randomly distributed connections, or by following a deterministic iterative rule for new nodes. The first procedure generates what is usually called a generalized random graph, while the latter was recently referred as deterministic scale-free network [37].

Deterministic scale-free networks are hierarchical structures composed by some succession of generations of nodes, i.e. the set of new nodes appearing simultaneously at a given iteration during the 'construction' of the network, whose connections follow a particular power-law distribution [37–40], being more easier to handle. The main difference between random and deterministic scale-free networks arises from the local connectivity character of the latter: random constructions generate irregular long-range connections, while deterministic networks impose a succession of generations of new nodes which are, in some way, organized in 'space'. Therefore, deterministic networks are applied for instance in spin systems [39], and geographical and social networks [39,41].

After considering separately dynamical and topological complexity, the next logical step toward real network dynamics is to consider them together. One important question addressed in this context is to know whether full synchronization between oscillators in such complex topologies would appear and under which conditions the full synchronized state would be stable. By full synchronization we mean the convergence of the amplitudes of all oscillators to the same value, evolving *coherently* from then on. Therefore we call henceforth these fully synchronized states *coherent states*, to distinguish them from *partially* synchronized configurations, when several different clusters of nodes with the same amplitude are observed [16]. Synchronization and coherent behaviour of oscillator networks with complex topologies have been studied for the random topology [42–45] and the small-world topology [46–49], and also scale-free networks [45,50–53]. In random networks, it is already known [42] that with high coupling strengths it is possible to fully synchronize oscillators and the corresponding stability condition may be computed [43] from the matrix of connections characterizing the network. In small-world networks, synchronizability is observed [47] only at the end of the small-world regime (high values of p), and recently [46] it was found that heterogeneity in the coupling may destroy coherence. These findings for small-world networks are somehow contradictory to the ones of other studies [45,48] and other topological quantifiers have been proposed [49]. In scale-free networks some recent studies indicate that synchronizability among oscillators depends on the average connectivity [52] and is robust to a delayed flow of information [50] and to the removal of low-connected nodes [52].

In this chapter we describe the general approach to study coherent states in any general complex network of oscillators, and apply it to the particular case of a scale-free network of discrete-time oscillators, which is studied in great detail. We start in Sect. 2 by describing the stability analysis approach to the model introduced in (1) and deduce the corresponding conditions for synchronizability. In Sect. 3 we apply this stability analysis procedure to the particular case of scale-free networks, comparing our results with numerical simulations. The random scale-free case is treated in Sect. 3.1, where we show that the threshold value of such a transition as a function of coupling

strength and outgoing connectivity obeys a power law with an exponent that depends on the nonlinearity, while deterministic scale-free networks are studied in Sect. 3.2, namely a pseudo-fractal network [38] and an Apollonian network [39, 40]. Discussion and conclusions are given in Sect. 4.

2 General Approach to Analyse Coherent States

For all the network topologies described above, if one considers discrete-time oscillators, namely maps of the interval, the equation of evolution for their amplitudes reads

$$\boldsymbol{x}_{t+1} = \boldsymbol{f}(\boldsymbol{x}_t) - \varepsilon \mathbb{G} \boldsymbol{g}(\boldsymbol{x}_t) \ , \tag{1}$$

where ε is the coupling parameter, t labels time, $\boldsymbol{x}_t = (x_{t,1}, \ldots, x_{t,N})$ with $x_{t,i}$ representing the amplitude at time-step t of node $i = 1, \ldots, N$, where N is the total number of nodes, $\boldsymbol{f} = (f(x_1), \ldots, f(x_N))$ and $\boldsymbol{g} = (g(x_1), \ldots, g(x_N))$ with f and g being real nonlinear functions, and $\mathbb{G}$ is the coupling (Laplacian) matrix, whose element G_{ij} represents the relative strength with which node i is coupled to node j, and satisfies the conditions $\sum_{j=1}^{N} G_{ij} = 0$ and $G_{ii} = 1$ for all $i = 1, \ldots, N$. In general $\mathbb{G}$ is a non symmetric matrix.

Usually, one chooses $\boldsymbol{g}(\boldsymbol{x}) \equiv \boldsymbol{x}$ when studying linear coupling, and $\boldsymbol{g}(\boldsymbol{x}) \equiv \boldsymbol{f}(\boldsymbol{x})$ when studying nonlinear coupling. Here we consider the nonlinear case. Apart from this choice, all the information about the dynamics is introduced in the function $\boldsymbol{f}(\boldsymbol{x})$, while all the information about the coupling topology (regular, random, small-world or scale-free) and the coupling regime (either homogeneous or heterogeneous) is included in the coupling matrix $\mathbb{G}$.

From (1) one easily sees that the coherent state $x_{t,1} = x_{t,2} = \cdots = x_{t,N} = X_t$ evolves in time according to the local map $X_{t+1} = f(X_t)$. There are two ways to study these coherent states: either by studying the stability of small perturbations of the coherent states or by making statistics over significant large samples of initial configurations, counting how many converge to a coherent state. Some attention to the parameter ranges must be taken, since the basin of attraction of the coherent states may be bounded by regions of phase space where amplitudes diverge. In particular, for maps of the interval one has $0 \leq \varepsilon \leq 1$ in order to guarantee convergence of any initial configuration.

In this chapter we shall illustrate both analytical and numerical approaches for the particular case of scale-free networks. To this end, we define the coupling matrix as $G_{ii} = 1$ and

$$G_{ij} = -\frac{k_j^{\alpha}}{\sum_{k \in \mathcal{K}_i} k_k^{\alpha}} \tag{2}$$

if node i is coupled to node j, with k_j representing the number of neighbours of node j and $\mathcal{K}_i$ is the set of labels of all neighbours of node i. If nodes i and j are not coupled $G_{ij} = 0$. The parameter α is a real number controlling

the heterogeneity in the coupling: positive values of α enhance the coupling strength with sites having a large number of neighbours, while negative values favour sites having less neighbours. For $\alpha = 0$ the coupling between each site and its neighbourhood is homogeneous.

For local dynamics we choose the well-known quadratic map $f(x) = 1 - ax^2$, where the free parameter a is restricted to the interval $-0.25 \leq a \leq 2$ and contains all possible dynamical regimes from a fixed point (e.g. $a = 0$) to fully developed chaotic orbits (e.g. $a = 2$).

When determining the stability of coherent states, various criteria are possible. For instance, one could compute the maximum Lyapunov exponent and obtain the conditions where it is negative. However, such a Lyapunov exponent does not indicate the existence of a local instability in the synchronous state, which may pull the trajectories apart from the coherent manifold.

The correct approach is based on the variational version of (1) proposed by Pecora and Carroll [54], which is valid for any network of identical oscillators as far as their local dynamics (quadratic map, Lorenz system, etc.) and their coupling regime (linear, nonlinear, etc.) are concerned. For the nonlinear coupling regime, the diagonal form of these variational equations reads [54–56]

$$\xi_{t+1,i} = \exp\left[\Lambda(\varepsilon\lambda_i)\right]\xi_{t,i} = \left[Df(X) - \varepsilon\lambda_i Df(X)\right]\xi_{t,i}\,, \tag{3}$$

for the coherent states $x_{t,i} = X$, where $\Lambda(\varepsilon\lambda_i)$ is the Lyapunov exponent, $Df(X)$ represents the identity matrix multiplied by the derivative of $f(x)$ computed at $x = X$ and λ_i are the eigenvalues of the coupling matrix $\mathbb{G}$. If $\mathbb{G}$ has zero-sum rows, i.e. $\sum_{j=1}^{N} G_{ij} = 0\,\forall i$, and all its eigenvalues $\lambda_1 \leq \lambda_2 \leq \cdots \leq \lambda_N$ are real and nonnegative, then $\lambda_1 = 0$ corresponds to the mode parallel to the synchronization manifold and the largest Lyapunov exponent defines a master stability function [54]. The coherent state is stable whenever $\Lambda(\varepsilon\lambda_i) < 0$ for $i = 2, \ldots, N$ [54–56].

In our case, it is easy to check from (2) that $\mathbb{G}$ has indeed zero-row sum, yielding $\lambda_1 = 0$. Moreover, all the eigenvalues of the matrix $\mathbb{G}$ are real and nonnegative, since $\det(\mathbb{G} - \lambda\mathbb{I}) = \det(\bar{\mathbb{G}} - \lambda\mathbb{I})$ where $\bar{\mathbb{G}}$ is a positive semidefinite symmetric matrix, namely $\bar{\mathbb{G}} = \mathbb{H}^{1/2}\mathbb{K}^{1/2}\mathbb{A}\mathbb{K}^{1/2}\mathbb{H}^{1/2}$ with $\mathbb{A}$ being the adjacency matrix of the network [52], and matrices $\mathbb{H}$ and $\mathbb{K}$ being the diagonal matrices with elements $H_{ii} = 1/(\sum_{k\in\mathcal{K}_i} k_k^{\alpha})$ and $K_{ii} = k_i^{\alpha}$ respectively.

From (3) and regarding the ordering of the eigenvalues λ_i one easily concludes that the stability condition reads

$$\varepsilon_L \equiv \frac{1 - \exp(-\bar{\lambda})}{\lambda_2} < \varepsilon < \frac{1 + \exp(-\bar{\lambda})}{\lambda_N} \equiv \varepsilon_U\,, \tag{4}$$

where $\bar{\lambda}$ is the Lyapunov exponent of the local single map. In particular there is a range of coupling strengths enabling synchronizability whenever $\lambda_N/\lambda_2 < (1+\mathrm{e}^{-\bar{\lambda}})/(1-\mathrm{e}^{-\bar{\lambda}})$ holds. Therefore, by computing the eigenvalues of the Laplacian matrix $\mathbb{G}$ one is able to find the range of couplings for which

coherent states are stable. This approach can be applied for any system ruled by (1).

3 Scale-Free Networks of Coupled Logistic Maps: An Example

For the particular case of scale-free networks, recent results [45] show a transition to full synchronization for two particular values of the nonlinearity a in the homogeneous regime ($\alpha = 0$), when either the coupling strength or the number of outgoing connections is varied. However, as far as we know there is no detailed study showing how these coherent states depend on all the model parameters. Therefore, we present in this section detailed numerical results concerning synchronization in oscillator networks with scale-free topologies. Our purpose is to give a complete example of how to study coherent solutions in complex networks of oscillators, comparing both the stability analysis and the numerical approaches.

The stability analysis is carried out just by computing the boundary values ε_L and ε_U in (4) as functions of the model parameters. The ranges of values where $\varepsilon_L < \varepsilon_U$ are the ones where coherent solutions appear. As stated above, for discrete oscillators, ruled by maps of the interval, the condition $0 \leq \varepsilon \leq 1$ must be added.

Numerically, to detect coherent solutions from a given sample of initial configurations, we compute the standard mean square deviation [45]

$$\sigma_t^2 = \frac{1}{N} \sum_{i=1}^{N} (x_{t,i} - \bar{x}_t)^2 \,, \tag{5}$$

where $\bar{x}_t$ is the average amplitude at a given time step t. Whenever σ^2 is zero within numerical precision, i.e. $\sigma^2 \sim 10^{-30}$, all the nodes are synchronized at the same amplitude.

We divide our approach into two parts, one concerning random scale-free networks (Sect. 3.1) and the other one concerning deterministic scale-free networks (Sect. 3.2).

3.1 Random Scale-Free Networks

In this section, we use the algorithm of Barabási and Albert [2, 30] to construct the random scale-free network (see Sect. 1), where at each node one places a chaotic logistic map. In a previous work [45] a transition to coherence between chaotic logistic maps was found for random scale-free networks, occurring for particularly high coupling strengths, typically of the order of $\varepsilon_c \sim 0.9$. Our simulations have shown that these transitions occur after discarding transients of $\sim 10^4$ time steps and they do not change significantly

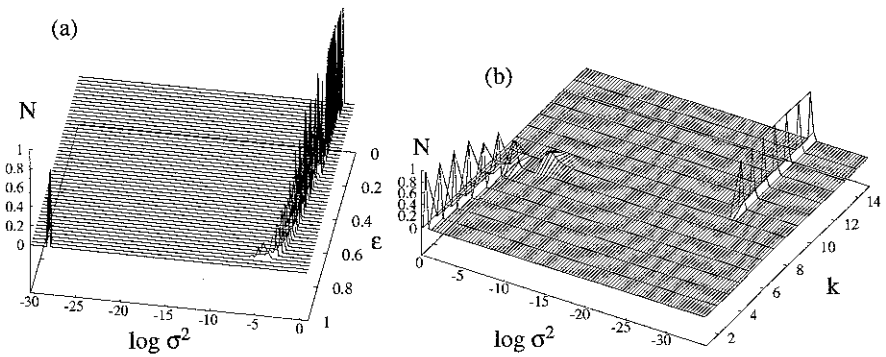

Fig. 1. Typical histograms of the standard mean square amplitude deviation σ^2 showing the sharp transition to coherence in function of **(a)** the coupling strength ε with $k = m_0 = 8$, and **(b)** the outgoing connectivity k with $\varepsilon = 0.95$. Values of N represent the fraction of configurations which converge to a coherent state from a total of 500 initial random configurations, after discarding transients of 10^4 time steps. Here $a = 2$, $N = 1000$, and $\alpha = 0$

with the network size. Moreover, as shown in Fig. 1, this transition to coherence is robust with respect to initial configurations, by varying either the coupling strength ε (Fig. 1a) or the outgoing connectivity k (Fig. 1b). In particular, above the threshold $\varepsilon_c \sim 0.9$, all initial configurations converge to a coherent state, indicating that in this parameter region the basin of attraction of coherent states fills almost the entire phase space.

From stability analysis, we find that in the fully chaotic regime ($a = 2$) the transition to coherence occurs for gradually smaller coupling strength if the connectivity k is increased. Figure 2a shows the boundaries ε_L and ε_U as a function of k for $a = 2$ (solid lines) and $a = 1.9$ (dashed lines) with the same parameter values as in Fig. 1. As one sees, in both cases the lower boundary ε_L decreases when k increases, while the upper boundary ε_U increases beyond $\varepsilon = 1$. Therefore, one expects that the region of synchronizability increases for larger values of connectivity k. Figure 2a also shows clearly that for $a = 2$ the intersection between both boundaries, $\varepsilon_L = \varepsilon_U$, occurs just above $k = 7$, which explains why the transition to coherence in Fig. 1b occurs at this value. For $a = 1.9$ this transition should occur near $k = 5$. Decreasing even more the nonlinearity coherent solutions are observed for even smaller connectivities and synchronizability regions increase, as shown in Fig. 2b. To see this feature more clearly we magnify in Fig. 2c the rectangle of Fig. 2b. As one sees, one exception occurs for $a = 1.8$, where the lower boundary is *below* the one for $a = 1.7$, due to the fact that for $a = 1.8$ the Lyapunov exponent of the logistic map is smaller than the one for $a = 1.7$, as illustrated below in Fig. 4. For all these values of a, the single uncoupled map shows chaotic orbits. Moreover, for any other network size N, the same curves are obtained.

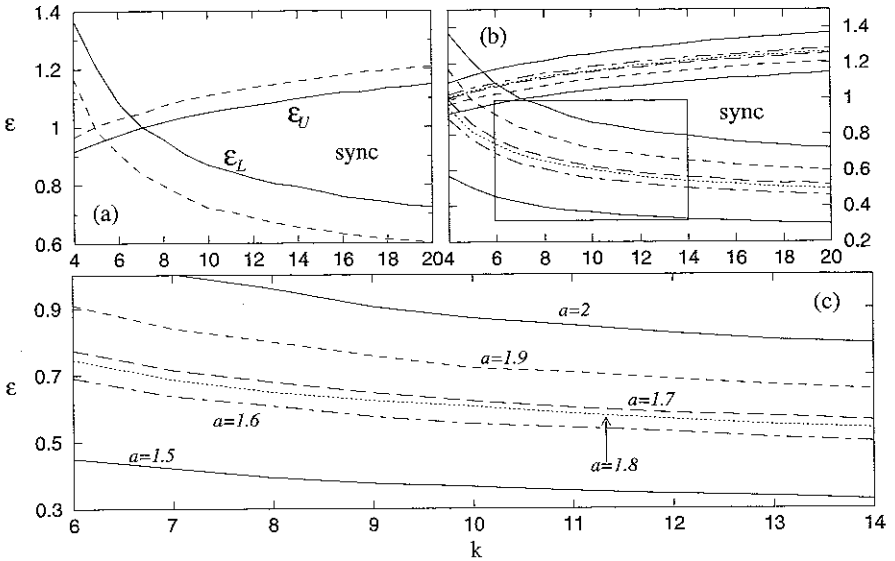

Fig. 2. Boundary values ε_L and ε_U in (4) in function of the connectivity k **(a)** for $a = 1.9$ (*dashed lines*) and $a = 2$ (*solid lines*), and **(b)** for $a = 1.5, 1.6, 1.7, 1.8, 1.9$ and 2. The data in the rectangle in **(b)** is magnified in **(c)**. The regions labelled with 'sync' are the ones where coherent solutions are observed, i.e. $\varepsilon_L < \varepsilon_U$. Notice that in (c) the boundary for $a = 1.8$ is below the one for $a = 1.7$, contrary to other values (see text)

These analytical predictions extracted from the stability condition in (4) and shown in Fig. 2 are strongly corroborated with our numerical simulations as shown in Fig. 3. In Fig. 3a we plot the fraction F of initial configurations which converge to a coherent state for $a = 2$, while Fig. 3b shows the threshold values, ε_c and k_c, at the transition curves where the entire sample of initial configurations converge to a coherent state, for the same values of a as in Fig. 2c. Here, one clearly sees that there is a clear and sharp transition to coherence. Interestingly, the curves in Fig. 3b fit very well the ones in Fig. 2c, which means that whenever the synchronizability condition $\varepsilon_L < \varepsilon_U$ holds, coherent states fill almost entirely the phase space.

Moreover, as illustrated in Fig. 3c, all curves obey a power law, within our numerical precision,

$$\varepsilon_c \propto k_c^{-\mu} \,. \tag{6}$$

For the six above values of a, the exponents are respectively $\mu = 0.2345$, 0.2354, 0.2353, 0.2231, 0.2023 and 0.1804: the exponent is almost constant below $a \sim 1.7$ and decreases above this value, as illustrated in the inset of Fig. 3c.

To determine the nature of the transition to coherence seen in Figs. 3a and 3b, we plot in Figs. 3d and 3e the average standard deviation in the

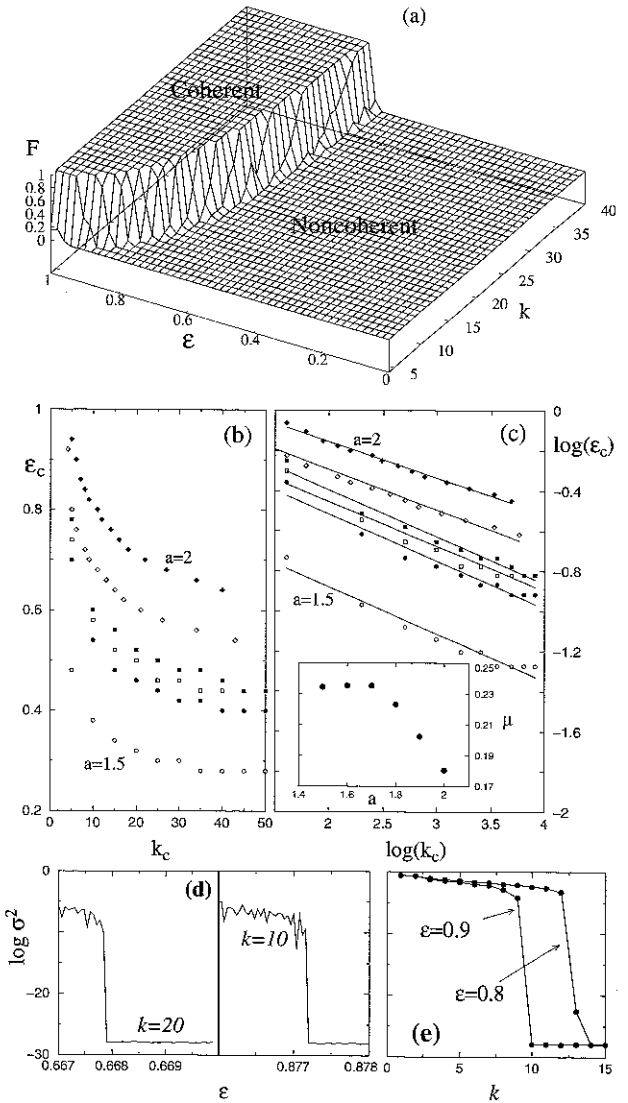

Fig. 3. Transition to coherence as a function of connectivity k and coupling strength ε. **(a)** Fraction $N_{\sigma=0}$ of coherent states from 500 random initial configurations for $a = 2$. **(b)** Coherence transition curves in the (ε, k) plane for (from bottom to top) $a = 1.5, 1.6, 1.8, 1.7, 1.9$ and $a = 2$, and **(c)** the same transition in a log-log plot, showing power-law dependence between connectivity and coupling strength for the transition curves, with an exponent μ which depends on the value of a (see inset). Here $\alpha = 0$, $L = 1000$ and we used transients of 10^4 time steps. By increasing the transient size to $\sim 10^6$ one clearly sees that the transition to coherence is of first-order either **(d)** when varying the coupling strength ε or **(e)** when varying the outgoing connectivity k

region where transition to coherence is observed, using much higher resolution. One clearly sees that the transition to coherence is of first-order, when varying ε or k. That the transitions are indeed of first order is easily recognised by the clear existence of hysteresis: when increasing either ε or k the configuration eventually falls into a coherent state, no longer spontaneously desynchronizing, no matter how far the parameters are tuned back.

All results till now, concern the case of homogeneous coupling ($\alpha = 0$). Next, we study the case of heterogeneous coupling. Figure 4 shows the boundaries ε_L and ε_U in (4) as functions of the outgoing connectivity k, the nonlinearity a and the heterogeneity α, covering both the homogeneous and heterogeneous regimes. Figure 4a shows the two boundaries as a function of k for $a = 2$ and $\alpha = 0$ (solid lines), $\alpha = 1$ (dashed lines) and $\alpha = 2$ (dotted lines). As one sees for nonzero values of α the boundaries are no longer smooth curves, but instead they show fluctuations as k is increased, enlarging and shrinking alternately the region of synchronizability, labelled as 'sync'. When varying a (Fig. 4b) the boundaries are mainly controlled by the Lyapunov exponent of the local map (see (4)), where ε_L (resp. ε_U) decreases (resp. increases) whenever a periodic window occurs [57]. The fluctuations observed in Fig. 4a are clearly seen in Fig. 4c, where the stability boundaries are plotted in function of α fixing $k = 8$ and $a = 2$ (solid lines) and $a = 1.5$ (dashed lines). The fluctuations are much higher for $\alpha > 1$ and for the fully chaotic regime both boundaries may even cross each other suppressing synchroniz-

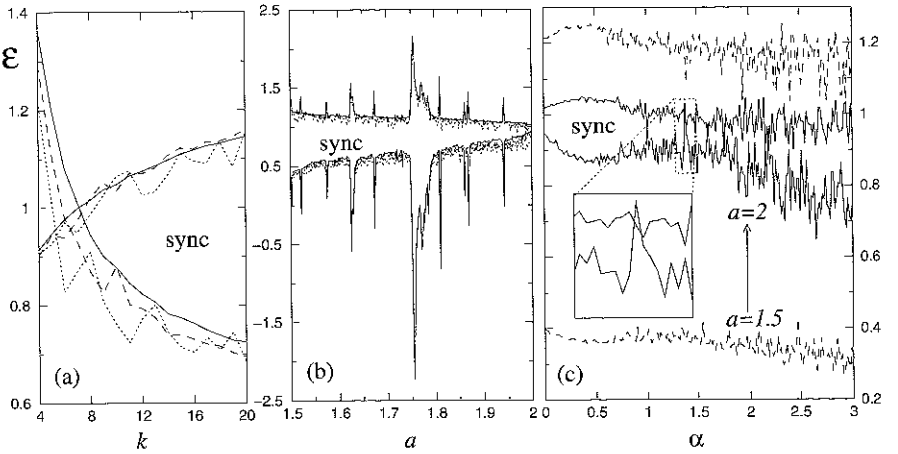

Fig. 4. Boundary values ε_L and ε_U in (4) in function of **(a)** connectivity k with $a = 2$ and $\alpha = 0$ (*solid lines*) $\alpha = 1$ (*dashed lines*) and $\alpha = 2$ (*dotted lines*), **(b)** nonlinearity a for $k = 8$ and $\alpha = 0, 1$ and 2, and **(c)** heterogeneity α with $k = 8$ and $a = 2$ (*solid lines*) and $a = 1.5$ (*dashed lines*). The inset in (c) emphasises one small region where synchronizability is not observed, $\varepsilon_L > \varepsilon_U$ (see text). Here $N = 1000$

ability (see inset of Fig. 4c). Moreover, the lower boundary ε_L decreases till $\alpha \sim 0.5$, then increases till $\alpha \sim 1$ and decreases in average from there on.

All these analytical results computed from (4) and matrix $\mathbb{G}$ in (1) are corroborated by our numerical simulations. In particular, the boundaries ε_L and ε_U seen in Fig. 4c are obtained also when plotting the contour of Fig. 5a, where we plot the average standard deviation from a sample of 500 initial configurations and vary the coupling strength and heterogeneity for $a = 2$ and $L = 1000$. While Fig. 5a shows the numerical results for $\alpha > 0$, i.e. in the case where nodes are more strongly coupled to the neighbours with higher connectivities, Fig. 5b shows the transition to coherence when $\alpha < 0$. Here synchronizability is observed only for $\alpha \gtrsim -0.15$ and for very high coupling strengths $\varepsilon \gtrsim 0.95$.

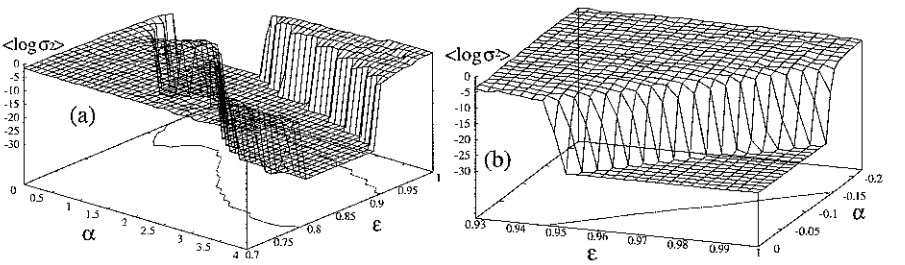

Fig. 5. Transition to coherence in function of coupling strength ε and heterogeneity α **(a)** when the most connected nodes dominate the dynamics ($\alpha > 0$) and **(b)** when the coupling to nodes with the least neighbours is strengthened ($\alpha < 0$). Here, we compute the average standard deviation from a sample of 500 initial configurations and fix $a = 2$, $k = m_0 = 8$ and $N = 1000$

We end our study of coherent solutions in random scale-free networks by investigating briefly the role of hubs in the lattice. Instead of strengthening the coupling to the most connected nodes by increasing $\alpha > 0$, we now fix $\alpha = 0$ and impose synchronization between all the nodes with more than a certain threshold k_t of neighbours and observe which fraction of the initial configurations converges to a coherent state. In this case the transition to coherence converges asymptotically to a limit of the coupling strength, as shown in Fig. 6a. The same occurs when synchronization is imposed to all nodes with *less* than k_t neighbours, as shown in Fig. 6b.

3.2 Deterministic Scale-Free Networks

In the previous section we focused on random scale-free networks, i.e. growing networks where new nodes are connected following probabilistic rules. In this section we study deterministic scale-free networks [37–39], using two different deterministic topologies: the pseudo-fractal scale-free network introduced by

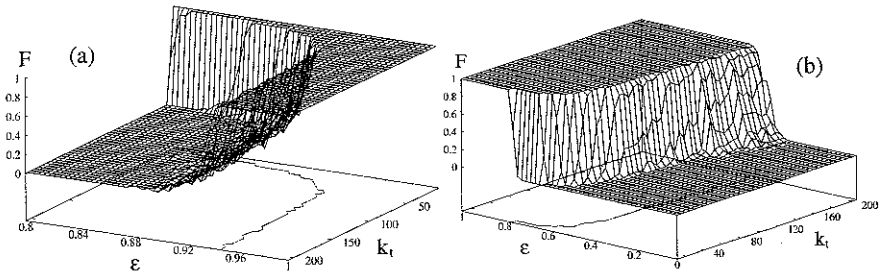

Fig. 6. Transition to coherence when synchronization is imposed to all nodes having a number of neighbours **(a)** larger than a threshold k_t, and **(b)** smaller than k_t (see text). Here $a = 2$, $k = 8$, $\alpha = 0$ and $N = 1000$

Dorogovtsev et al [38] and the Apollonian network introduced by Andrade et al. [39] and also studied in [40]. Both networks are illustrated in Fig. 7.

The pseudo-fractal network of Dorogovtsev is obtained, starting from three interconnected nodes, and at each iteration each edge generates a new node, attached to its two vertices. Figure 7a illustrates this network after three iterations, i.e. with three generations of nodes. The number of nodes N_n and the number of connections V_n increase with the number of generations as [38]

$$N_n = \tfrac{3}{2}(3^n + 1)\,, \tag{7a}$$

$$V_n = 3^{n+1}\,. \tag{7b}$$

From Fig. 7a one easily sees that this network has indeed a scale-free topology, since the number of nodes with degree $k = 2, 2^2, \ldots, 2^{n-1}, 2^n$ and 2^{n+1} is equal to $3^n, 3^{n-1}, \ldots, 3^2, 3$ and 3 respectively. In particular, the exponent of this power-law distribution is $\gamma = 1 + \ln 3/\ln 2$. Moreover, the cluster

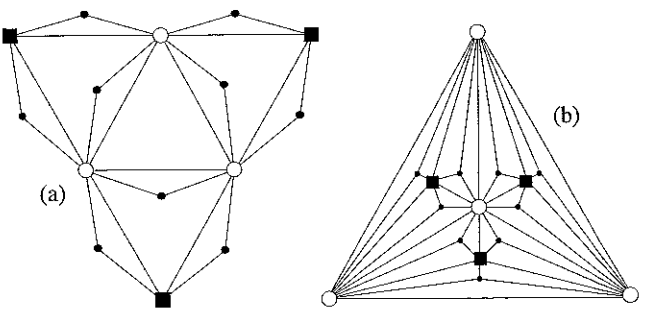

Fig. 7. Illustrations of two deterministic scale-free networks: **(a)** the pseudo-fractal network [41], and **(b)** the Apollonian network [39]. Identical symbols label nodes belonging to the same generation n (see text), namely ○ for $n = 0$, ■ for $n = 1$ and • for $n = 2$

coefficient of a node with degree k is $C = 2/k$, and the average path length is approximately $\langle \ell \rangle \simeq 4 \ln N_n / (9 \ln 3)$.

The Apollonian network is constructed in a different way: one starts with three interconnected nodes, defining a triangle; at $n = 0$ one puts a new node at the center of the triangle and joins it to the three other nodes, thus defining three new smaller triangles; at iteration $n = 1$ one adds at the center of each of these three triangles a new node, connected to the three vertices of the triangle, defining nine new triangles and so on (see Fig. 7b). The number of nodes and the number of connections are respectively given by

$$N_n = \tfrac{1}{2}(3^{n+1} + 5) \,, \tag{8a}$$

$$V_n = \tfrac{3}{2}(3^{n+1} + 1) \,. \tag{8b}$$

The distribution of connections obeys a power law, since the number of nodes with degree $k = 3, 3 \times 2, 3 \times 2^2, \ldots, 3 \times 2^{n-1}, 3 \times 2^n$ and 2^{n+1} is equal to $3^n, 3^{n-1}, 3^{n-2}, \ldots, 3^2, 3, 1$ and 3 respectively, and the exponent γ is the same as for the pseudo-fractal network. Moreover, a node with k neighbours has a cluster coefficient of $C \simeq 4/k$ as reported in [40], converging on average to $C_\infty = 0.828$, and the average path length grows weaker than $\ln N_n$ [39].

Although both networks have similar values for the topological quantities, they are quite different from the geometrical point of view: the pseudo-fractal network has no metric, while the Apollonian network is embedded in Euclidean space and fills it densely as $n \to \infty$, being particularly suitable to describe geographical situations [39].

For stability analysis purposes (see Sect. 2), the Laplacian matrix $\mathbb{G}$ of deterministic networks can be analytically determined from the adjacency matrix $\mathbb{A} = \{a_{ij}\}$, since they are related by

$$\mathbb{G} = \mathbb{I} + \mathbb{A}\mathbb{T} \,, \tag{9}$$

where $\mathbb{I}$ is the identity matrix and the values of matrix $\mathbb{T} = \{T_{ij}\}$ are defined by

$$T_{ij} = -\frac{a_{ji} \left[\sum_{k=1}^{N} a_{ik}\right]^{\alpha}}{\sum_{p=1}^{N} a_{jp} \left[\sum_{k=1}^{N} a_{pk}\right]^{\alpha}} \,. \tag{10}$$

A simple way to write the adjacency matrix of the pseudo-fractal network is

$$\mathbb{A}_n = \begin{bmatrix} \mathbb{A}_{n-1} & \mathbb{M}_{n-1} \\ \mathbb{M}_{n-1}^T & \emptyset \end{bmatrix}_{N_n \times N_n} \,, \tag{11}$$

where N_n is given by (7a), $\mathbb{M}^T$ represents the transposed matrix of $\mathbb{M}$ and for each generation $n = 1, 2, \ldots$ the matrix $\mathbb{M}_n$ reads

$$\mathbb{M}_n = \begin{bmatrix} \mathbb{M}_{n-1} & \mathbb{M}_{n-1} & \emptyset \\ \emptyset & \emptyset & \mathbb{B}_{n-1} \end{bmatrix}_{(2 \times 3^{n-1}) \times 3^n} \,, \tag{12}$$

with

$$\mathbb{B}_{n-1} = \begin{bmatrix} \mathbb{A}_0 & \emptyset & \dots & \emptyset \\ \emptyset & \mathbb{A}_0 & \dots & \emptyset \\ \vdots & \vdots & \ddots & \vdots \\ \emptyset & \emptyset & \dots & \mathbb{A}_0 \end{bmatrix}_{3^{n-1}\times 3^{n-1}} \tag{13}$$

and whose starting form is

$$\mathbb{M}_0 = \mathbb{A}_0 = \begin{bmatrix} 0\,1\,1 \\ 1\,0\,1 \\ 1\,1\,0 \end{bmatrix}_{3\times 3} . \tag{14}$$

For the Apollonian network, the adjacency matrix is given by the same recurrence of (11), but this time with

$$\mathbb{A}_0 = \begin{bmatrix} 0\,1\,1\,1 \\ 1\,0\,1\,1 \\ 1\,1\,0\,1 \\ 1\,1\,1\,0 \end{bmatrix} , \tag{15}$$

and $\mathbb{M}_n$ being a matrix with $(3^n + 5)/2$ rows and 3^n columns and having in each column only three nonzero elements.

Figure 8 shows the eigenspectra of the Laplacian matrices for both the pseudo-fractal (Fig. 8a) and the Apollonian (Fig. 8b) networks, in function of the heterogeneity. As one sees for $a = 2$ (solid lines) synchronizability is observed only above $\alpha \gtrsim 1.5$, and in particular there is no synchronizability for the homogeneous coupling regime ($\alpha = 0$). Figure 9a shows the distribution of the average standard deviation over a sample of 500 initial configurations, from which one clearly sees that there are no coherent solutions. Here the standard mean deviation is characterized by some large value which is almost constant beyond the weak coupling regime ($\varepsilon \gtrsim 0.2$). In the weak coupling regime ($\varepsilon \lesssim 0.2$) the standard mean square deviation is even larger, since the coupling is not strong enough to compensate the highly chaotic local dynamics ($a = 2$).

From Fig. 8 one also sees that, for the pseudo-fractal and $\alpha > 1.5$, the upper threshold ε_U increases monotonically with the heterogeneity, while for the Apollonian network the upper threshold decreases. This particular difference between both networks should be due to their geometrical differences, in particular the fact that Apollonian networks are embedded in Euclidean space could explain in some way that stronger dominance in the coupling to the most connected nodes *destroys* coherence.

Choosing other values of a for which the local dynamics is chaotic, one finds that the form of de curves $\varepsilon_L(\alpha)$ and $\varepsilon_U(\alpha)$ does not change. These curves are only shifted: ε_L gets smaller, while ε_U increases. Figure 8 illustrates this for the particular case of $a = 1.5$. Decreasing even further the nonlinearity

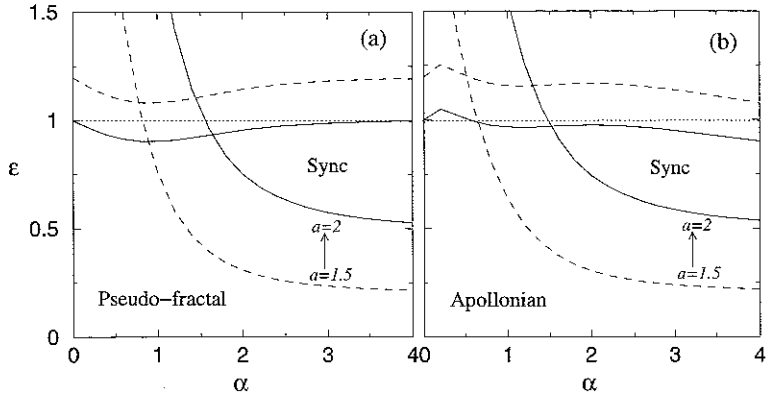

Fig. 8. Boundary ε_L and ε_U for synchronizability in function of the heterogeneity α for **(a)** the pseudo-fractal network and **(b)** the Apollonian network, with $a = 2$ (*solid lines*) and $a = 1.5$ (*dashed lines*). For each network we use 6 generations of nodes (see text). These eigenspectra are the same for any number of generations

below the accumulation point $a = 1.411\ldots$ synchronizability is attained for any positive value of α, whenever the coupling strength is sufficiently strong.

Moreover there is a complicated dependence of the average standard deviation on the coupling strength and nonlinearity. As shown in Fig. 9b for deterministic scale-free networks one finds two main regions in the (a, ε) plane: (I) a region where the standard mean square deviation is large and varies

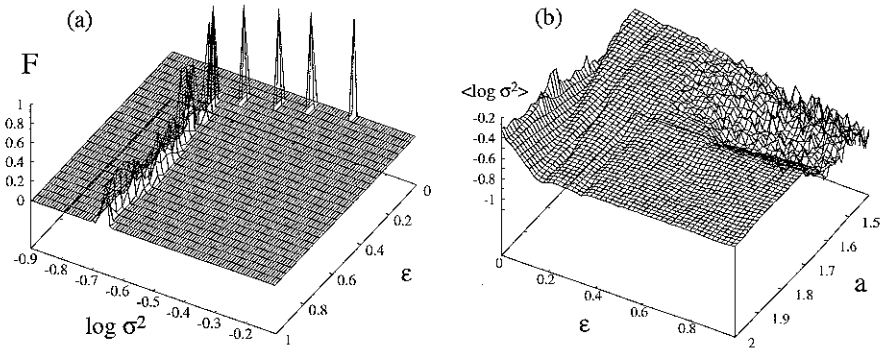

Fig. 9. (a) Typical histogram of the standard mean square deviation σ^2 for the pseudo-fractal network as a function of the coupling strength ε, with $a = 2$ and $\alpha = 0$. A similar result is obtained for the Apollonian network. **(b)** Histogram of the standard mean square deviation σ^2 as a function of nonlinearity a and coupling strength ε, for deterministic scale-free networks with $\alpha = 0$. The mean square deviation is averaged over a sample of 500 initial configurations and during 100 time steps, after discarding transients of 10^4 time steps

smoothly with the parameters and (II) a region where the mean square deviation is smaller but has larger fluctuations. This second region, observed for $a \lesssim 1.7$, is somehow surprising, since irregular variations of the standard mean square deviation occur for low nonlinearity and high coupling strengths, precisely where one would expect the most regular behaviour of the node dynamics.

As for the heterogeneous coupling regime ($\alpha \neq 0$), Fig. 10 illustrates the transition to coherence by varying the heterogeneity α for the pseudo-fractal (Fig. 10a) and the Apollonian network (Fig. 10b). For both networks, one sees that coherence sets in for $\alpha \gtrsim 1.5$, and the contour of the histograms marking the transition to coherence fits well the regions in Fig. 8 labelled as 'sync'. Moreover, from Figs. 10c and 10d one observes that all these transitions to coherence are of first-order.

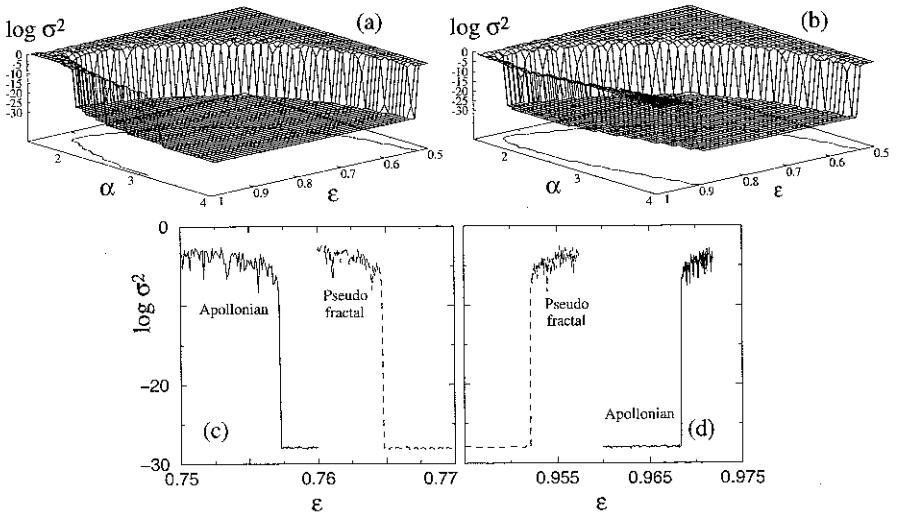

Fig. 10. Inducing transition to coherence by varying the heterogeneity α (see (1)) in scale-free networks. **(a)** Pseudo-fractal network and **(b)** Apollonian network. For strong heterogeneity coherence appears beyond a relatively high coupling strength, and disappears again for very large couplings (see text). For each network, we use $\ell = 6$ generations of nodes and fix $a = 2$. **(c)** and **(d)** show high-resolution plots of σ^2 as a function of ε for $\alpha = 2$, emphasizing the first-order phase transition to coherence

Finally, we study the role of hubs in deterministic scale-free networks, as we did in the previous section for random networks. To this end, we impose synchronization among $g = 1, \ldots, \ell$ generations, with ℓ being the total number of generations, and observed in what conditions coherent states are observed. In the pseudo-fractal network the first generation has $N_1 - N_0 = 3$ nodes, the second one has $N_2 - N_1 = 9$ nodes, and the nth generation has

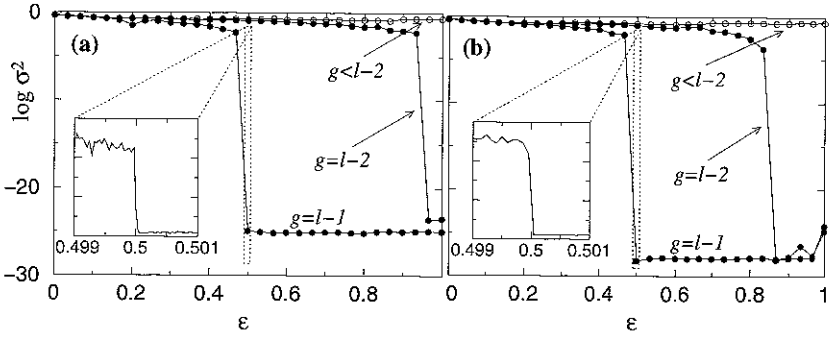

Fig. 11. Transitions to coherence in deterministic scale-free networks, when synchronizing the first g generations of nodes out of ℓ generations (see text). **(a)** Pseudo-fractal network and **(b)** Apollonian network. The collective dynamical behaviour is quite insensitive to hubs (see text). Insets show that transitions to coherence are of first-order. For each network, we use $\ell = 9$ generations of nodes and $a = 2$ fixed

$N_n - N_{n-1} = 3^n$ nodes. In the Apollonian network the number of nodes appearing at each generation is precisely the same.

Figure 11 shows the standard mean square deviation as a function of coupling strength for pseudo-fractal (Fig. 11a) and Apollonian networks (Fig. 11b). In each case we choose the fully chaotic map ($a = 2$) and impose synchronization among the nodes of the first g generations by setting them to their mean amplitude at each time-step. In both cases, one sees that the standard mean square deviation remains large when synchronization is imposed to all $g < \ell - 2$ generations. Coherent solutions are only observed for $g = \ell - 2$ and $g = \ell - 1$, beyond a coupling threshold which is smaller for the latter case. Surprisingly, for $g = \ell - 1$ the transition to coherence occurs for the same coupling strength in both networks. This may be due to the fact that the fraction $N_g/N_\ell = 3^{g-\ell} = 1/3$ of nodes on which one imposes synchronization is the same for both networks and is high enough to suppress the influence of local connectivities.

For $g = \ell - 2$ the pseudo-fractal network shows coherence only above very high coupling strengths, near $\varepsilon \sim 1$, while for Apollonian networks the threshold is much lower. This difference in the coupling strength threshold is due to the fact that here the fraction of nodes $N_g/N_\ell = 1/9$ to which synchronization is imposed is small enough not to suppress the influence of local connectivities. Therefore, since the hubs in the pseudo-fractal network are less connected than the hubs in Apollonian networks, one needs higher coupling strength to observe coherence. For any higher value ℓ of generations the same results are obtained, since one has for the quotient of the number of nodes between two successive generations $N_n/N_{n-1} \to 3$ as n increases.

As a general remark, one observes from Fig. 11 that one needs to synchronize a rather high fraction of nodes ($\gtrsim 1/9$) to induce coherence. Therefore, it seems that, dynamical collective behaviour on scale-free networks is quite insensitive to hubs. As shown in the insets of Figs. 11a and 11b, the transition to coherence is also of first-order.

4 Discussion and Conclusions

In this chapter we studied fully synchronized solutions for three scale-free network topologies. The main conclusion is the following: in random scale-free networks synchronization of chaotic maps not only depends on the coupling strength but is mainly controlled by the outgoing connectivity k, which is a measure of the cohesion in the networks. Because of that, one finds coherent solutions in random scale-free networks of fully chaotic logistic maps ($a = 2$) with outgoing connectivity $k = 8$ and homogeneous coupling, but not in deterministic scale-free networks, since they have rather small effective outgoing connectivity, namely $k = 2$ for the pseudo-fractal network and $k = 3$ for the Apollonian network. Therefore, although the exponent γ of connection distributions in scale-free networks does not depend on the outgoing connectivity [2], we have shown that, in general, synchronization of chaotic maps in such coupling topologies is quite sensitive to it.

Our results were obtained both numerically, from histogram of significantly large samples of initial configurations with a criterion for full synchronization based on the mean standard deviation of amplitudes, (5), and analytically from the eigenvalue spectra of the diagonalized variational equations computed at the coherent states, (3).

In particular, for random scale-free networks, the threshold values of the coupling strength obey a power law, (6), as function of the outgoing connectivity. The exponent of this power law depends on the nonlinearity a of the chaotic map, being almost constant below $a_c \sim 1.7$ and decreasing linearly above it. Interestingly this value of a_c is in the vicinity of the bifurcation of the quadratic map where the period-3 window appears, and coincides with the appearance of other nontrivial behaviours in coupled map lattices with regular topologies, namely in the velocity distribution of travelling wave solutions [24].

For deterministic scale-free networks with homogeneous coupling, the same value a_c indicates the threshold above which no coherent solutions are observed, independently of the coupling strength. Above a_c, coherence is observed only for heterogeneous coupling, namely for $\alpha \gtrsim 1.5$. However, for this range of values, we have also shown that coherence is also absent either for very small or for very large coupling strengths, due to spatial instabilities. Another particularly interesting result that still needs to be explained is that, for Apollonian networks, the coupling threshold beyond which coherence disappears gets smaller when the heterogeneity is further increased.

This point is not observed for the pseudo-fractal network and may be due to the geometrical differences between both deterministic networks.

As a general property, we have shown that all transitions to coherence are of first-order, indicating a similarity with other complex networks [29]. Furthermore, all results are robust not only against changes of the initial configurations of node amplitude but also, in random scale-free networks, against changes of the connection network. We also presented results indicating that in scale-free networks hubs play apparently no fundamental role in the dynamical collective behaviour.

Acknowledgments

The authors thank A.O. Sousa and C. Zhou for useful discussions. P.G.L. thanks Fundação para a Ciência e a Tecnologia, Portugal, for financial support. J.A.C.G. thanks Conselho Nacional de Desenvolvimento Científico e Tecnológico, Brazil and Sonderforschungsbereich 404 of DFG for financial support.

References

1. S. Bornholdt, H.G. Schuster (eds.): *Handbook of Graphs and Networks* (Wiley-VCH, Weinheim 2003)
2. R. Albert, A.-L. Barabási: Rev. Mod. Phys. **74**, 47 (2002).
3. S.N. Dorogovtsev, J.F.F. Mendes: Adv. Phys. **51**, 1079 (2002)
4. R. Meucci, R. McAllister, R. Roy: Phys. Rev. E **66**, 026216 (2002)
5. J.H. Snoeijer, T.J.H. Vlugt, M. van Hecke, W. van Saarloos: Phys. Rev. Lett. **92**, 054302 (2004)
6. M. Otto, J.-P. Bouchaud, P. Claudin, J.E.S. Socolar: Phys. Rev. E **67**, 031302 (2003)
7. C. Texier, G. Montambaux: Phys. Rev. Lett. **92**, 186801 (2004)
8. H. Tanaka, J. Meunier, D. Bonn: Phys. Rev. E **69**, 031404 (2004)
9. D.P. Almond, C.R. Bowen: Phys. Rev. Lett. **92**, 157601 (2004)
10. M. Small, C.K. Tse, Phys. Rev. E **66**, 066701 (2002)
11. I. Stewart: Nature **427**, 601 (2004)
12. Y. Moreno, M. Nekovee, A. Vespignani: Phys. Rev. E **69**, 055101(R) (2004)
13. Z. Dezso, A.L. Barabási: Phys. Rev. E **65**, 055103 (2002)
14. M. Compiani, E. Capriotti, R. Casadio: Phys. Rev. E **69**, 051905 (2004)
15. L. Zhaoping, A. Lewis, S. Scarpetta: Phys. Rev. Lett. **92**, 198106 (2004)
16. P.G. Lind, J. Corte-Real, J.A.C. Gallas: Phys. Rev. E **69**, 026209 (2004)
17. S.H. Strogatz: Physica D **143**, 1 (2000)
18. L.M. Pecora, T.L. Carroll, G.A. Johnson, D.J. Mar, J.F. Heagy: Chaos **7**, 520 (1997)
19. C. Anteneodo, A.M. Batista, R.L. Viana: Phys. Lett. A **326**, 227 (2004)
20. M. Cross, P. Hohenberg: Rev. Mod. Phys. **65**, 851 (1993)

21. K. Kaneko, I. Tsuda: *Chaos and Beyond* (Springer-Verlag, Berlin Heidelberg New York 2000)
22. S. Wolfram: *A New Kind of Science* (Wolfram Media Inc., New York 2002)
23. K. Kaneko (ed.): *Theory and Applications of Coupled Map Lattices* (John Wiley & Sons Inc., New York Chichester 1993)
24. P.G. Lind, J. Corte-Real, J.A.C. Gallas: Phys. Rev. E **69**, 066206 (2004)
25. S. Boccaletti, J. Kurths, G. Osipov, D.L. Valladares, C.S. Zhou: Phys. Rep. **366**, 1 (2002)
26. P. Erdös, A. Rényi: Publ. Math. Debrecen **6**, 290 (1959)
27. B. Bollobás: *Random Graphs* (Academic, London 1985)
28. D.J. Watts, S.H. Strogatz: Nature **393**, 440 (1998)
29. S.H. Strogatz: Nature **410**, 268 (2001)
30. A.-L. Barabási, R. Albert: Science **286**, 509 (1999)
31. K. Christensen, R. Donangelo, B. Koiler, K. Sneppen: Phys. Rev. Lett. **81**, 2380 (1998)
32. M.E.J. Newman, D.J. Watts: Phys. Rev. E **60**, 7332 (1999)
33. A.-L. Barabási, R. Albert, H. Jeong: Physica A **272**, 173 (1999)
34. S.N. Dorgovtsev, J.F.F. Mendes, A.N. Samukhin: Phys. Rev. Lett. **85**, 4633 (2000)
35. L. Kullmann, J. Kertész: Phys. Rev. E **63**, 051112 (2001)
36. P.L. Krapivsky, S. Redner, F. Leyvraz: Phys. Rev. Lett. **85**, 4629 (2001)
37. A.-L. Barabási, E. Ravasz, T. Vicsek: Physica A **299**, 559 (2001)
38. S.N. Dorogovtsev, A.V. Goltsev, J.F.F. Mendes: Phys. Rev. E **65**, 066122 (2002)
39. J.S. Andrade Jr, H.J. Herrmann, R.F.S. Andrade, L.R. da Silva: Phys. Rev. Lett. **94**, 018702 (2005)
40. J.P.K. Doye, C.P. Massen: Phys. Rev. E **71**, 016128 (2005)
41. M.C. González, A.O. Sousa, H.J. Herrmann: Int. J. Mod. Phys. C **15**, 45 (2004)
42. H. Chaté, P. Manneville: Chaos **2**, 307 (1992)
43. P.M. Gade: Phys. Rev. E **54**, 64 (1996)
44. S.C. Manrubia, A.S. Mikhailov: Phy. Rev. E **60**, 1579 (1999)
45. J. Jost, M.P. Joy: Phys. Rev. E **65**, 016201 (2001)
46. T. Nishikawa, A.E. Motter, Y.-C. Lai, F.C. Hoppensteadt: Phys. Rev. Lett. **91**, 014101 (2003)
47. M. Barahona, L.M. Pecora: Phys. Rev. Lett. **89**, 054101 (2002)
48. L.F. Lago-Fernández, R. Huerta, F. Corbacho, J.A. Siguenza: Phys. Rev. Lett. **84**, 2758 (2000)
49. H. Hong, B.J. Kim, M.Y. Choi, H. Park: Phys. Rev. E **69**, 067105 (2004)
50. F.M. Atay, J. Jost, A. Wende: Phys. Rev. Lett. **92**, 144101 (2004)
51. X.F. Wang, G. Chen: IEEE Trans. Circ. Sys. I **49**, 54 (2002)
52. A.E. Motter, C. Zhou, J. Kurths: Europhys. Lett. **69**, 334 (2005)
53. P.G. Lind, J.A.C. Gallas, H.J. Herrmann: Phys. Rev. E **70**, 056207 (2004)
54. L.M. Pecora, T.L. Carroll: Phys. Rev. Lett. **80**, 2109 (1998)
55. K.S. Fink, G. Johnson, T. Carroll, D. Mar, L. Pecora: Phys. Rev. E **61**, 5080 (2000)
56. S.C. Manrubia, A.S. Mikhailov, D.H. Zanette: *Emergence of Dynamical Order Synchronization Phenomena in Complex Systems, vol. 2* (World Scientific, Singapore 2004)
57. E. Ott: *Chaos in Dynamical Systems* (Cambridge University Press, New York 1993)
58. A. Pikovsky, O. Popovych, Yu. Maistrenko: Phys. Rev. Lett. **87**, 044102 (2001)